

This is an author-deposited version of the article.

To link to this article: DOI: 10.1021/cm4007298

URL: <https://doi.org/10.1021/cm4007298>

This article may be used for non-commercial purposes in accordance with ACS Sharing Policies.

This is the submitted manuscript. Supplementary Materials accompanying this article can be found on-line at the publisher's site.

Magnetic bioactive and biodegradable hollow Fe-doped hydroxyapatite coated poly(L-lactic) acid micro-nanospheres for medical applications

Michele Iafisco^{†*}, Monica Sandri[†], Silvia Panseri^{†‡}, José Manuel Delgado-López[§], Jaime Gómez-Morales[§] and Anna Tampieri[†]

[†]Laboratory of Bioceramics and Bio-hybrid Composites, Institute of Science and Technology for Ceramics (ISTEC), National Research Council (CNR), Via Granarolo 64, 48018 Faenza (Italy)

[‡]Laboratory of Biomechanics and Technology Innovation, Rizzoli Orthopaedic Institute, Via di Barbiano 1/10, 40136 Bologna (Italy)

[§]Laboratorio de Estudios Cristalográficos, IACT (CSIC-UGR), Av. Las Palmeras 4, E-18100 Armilla (Spain)

KEYWORDS: *hydroxyapatite, magnetism, microspheres, nanoparticles, poly(L-lactic) acid.*

ABSTRACT: Superparamagnetic iron-substituted hydroxyapatite nanocrystals (FeHA) were used as particulate emulsifier for the preparation of hybrid polymeric-inorganic materials by Pickering emulsion. As result, magnetic hollow micro-nanospheres (ranging from 2 μm to 500 nm) made of polymeric shell of poly(L-lactic) acid coated with FeHA have been prepared. Several hybrid composites containing different amounts of inorganic phase loaded to the polymeric shell were prepared. The amount of FeHA strongly affected the chemical-physical features of the spheres such as size, polymer crystallinity, surface charge and magnetization. They displayed good biocompatibility toward bone marrow mesenchymal stem cells and the spheres coated with higher amount of FeHA exhibited better cell proliferation than those coated with lower amount. These magnetic materials have potential uses as building blocks for the preparation of scaffolds for hard tissue regeneration as well as carriers of biomolecules for nanomedical applications.

Introduction

Nowadays, magnetic materials are receiving special attention due to their potential applications in different fields and in particular in medicine.^{1, 2} Magnetic micro-nano-particles have been progressively employed as support materials for enzyme immobilization, drug-delivery vehicles, contrast agents for magnetic resonance imaging, heat mediators for hyperthermia-based anti-cancer treatments and many other exciting biomedical applications.³⁻⁵ Magnetic materials have also recently attracted a big interest in the field of bone tissue regeneration because it has been demonstrated that magnetic nanoparticles have effect of osteoinduction even without external magnetic force.⁶ Magnetic scaffolds may provide great potential in bone regenerative medicine, in fact several papers reported that the introduction of magnetic nanoparticles to calcium phosphates bioceramics could promote bone formation and cell growth *in vitro* and *in vivo*,⁷ and that the same addition in hydroxyapatite-polymeric nanofibrous membranes could induce a significantly higher adhesion, proliferation rate and faster differentiation of osteoblast cells.^{8, 9} Therefore, one of the biggest challenges in this field is the production of magnetic materials with good biocompatibility and biodegradability. Iron oxide (magnetite or maghemite) is the most popular magnetic phase used in medicine and biotechnology^{10, 11} whose long-term effects in the human body are not yet completely assessed.^{12, 13} These materials are classified as “superparamagnetic”, indicating their ability to become magnetized upon exposure to a magnetic field without showing permanent magnetization

(remanence) once it is turned off.¹⁴ This ability is used in medicine as an efficient tool to move particles into the body towards target organs.¹⁵ To reduce their toxicity the surface of magnetic particles has been modified through the creation of biocompatible layers made of organic polymers, inorganic phases or metals deposited on the surface.¹⁶ Recently Tampieri et al.¹⁷ developed an innovative biocompatible and bioresorbable superparamagnetic-like phase by doping nano-hydroxyapatite with $\text{Fe}^{2+}/\text{Fe}^{3+}$ ions (FeHA), avoiding the presence of poorly tolerated magnetic secondary phases. They observed that a defined occupation of the crystal sites in the apatite lattice by the two iron species and that their unambiguous spatial distribution is mandatory condition for the expression of magnetic properties and hyperthermia. *In vitro* study showed that the novel FeHA nanoparticles not only did not reduce cell viability, but they enhanced cell proliferation compared to hydroxyapatite particles controls already used in clinical application. This positive effect was even significantly increased when a magnetic field was applied.¹⁸ Moreover a pilot animal study of bone repair (a rabbit critical bone defect model) demonstrated the *in vivo* biocompatibility and biodegradability of FeHA.¹⁸

Using the same approach, in this paper the preparation and characterization of magnetic FeHA nano-apatites coated hollow poly(L-lactic) acid micro-nanospheres are reported. Polymer-hydroxyapatite composites can combine better mechanical properties and flexibility than the single counterparts along with good bioactivity, biocompatibility and biodegradability.¹⁹

Scaffolds comprising micro- and nanospheres (spheres used as discrete components embedded into continuous matrices or as building blocks for bottom-up preparation of scaffolds) display several advantages in comparison with traditional monolithic ones e.g., (i) improving control over sustained delivery of therapeutic agents, signaling biomolecules and even pluripotent stem cells, (ii) serving as stimulus-sensitive delivery carriers for triggered release, (iii) introducing porosity and/or improve the mechanical properties of bulk scaffolds by acting as porogen or reinforcement agent, (iv) supplying compartmentalized micro-reactors for dedicated biochemical processes, (v) functioning as cell delivery vehicle, and (vi) giving possibility of preparing injectable and/or mouldable formulations to be applied by using minimally invasive surgery.²⁰ The micro-nanospheres were prepared using the Pickering emulsion. By definition, Pickering emulsions are solid particle-stabilized emulsions in the absence of any molecular surfactant, where solid particles adsorbed to an oil-water interface.²¹ Although this area of research rested inactive for many years, recently there has been increasing interest in this methodology because the absence of surfactants is very important in the preparation of biomedical materials since usually the surfactants are undesirable substances because they could be non-biodegradable and may cause allergic reactions and even tumors. A wide range of particles such as silica, metals, cellulose, apatite, starch, clays, micro-gels, and polystyrene latexes have been recently reported to be effective Pickering emulsifiers.²²⁻²⁹

Poly(L-lactic) acid has been used because poly(α -hydroxyesters), such as poly(lactic acid) (PLLA), poly(glycolic acid) (PGA), poly(lactic-co-glycolic acid) (PLGA), and poly(caprolactone) (PCL), are the most used synthetic polymers for biomedical applications owing to their biocompatibility, hydrolytic degradation process, proper mechanical properties and ease of manufacture.³⁰

The new magnetic hybrid material showed in this paper could represent, by virtue of its chemical-physical and morphological properties, a building block for the preparation of new type of scaffold for hard tissue regeneration as well as a drug-carrier for nanomedical applications. The magnetic functionality could allow to control the position of the nanocarriers inside the body by an external magnetic field and to use them for bioimaging applications.³¹ Furthermore, the magnetic feature of the nanoparticles could allow to tailor the release of the therapeutic agent by switching (on-off) the external magnetic field.³²

Experimental

Materials. Common high-purity chemical reagents were purchased from Sigma Aldrich (Milan, Italy). Poly(L-lactic) acid (PLLA) (Lacea H.100-E) was purchased from Mitsui Fine Chemicals (Dusseldorf, Germany) (Mn = 49400, Mw/Mn = 1.70). Ultrapure water (0.22 mS, 25 °C) was used in all the experiments. α -MEM medium, Fetal Bovine Serum (FBS) Penicillin-Streptomycin were purchased from PAA (Pasching, Austria). MTT reagent (3-(4,5-dimethylthiazol-2-yl)-2,5-diphenyltetrazolium bromide), DAPI (4',6-diamidino-2-phenylindole) and FITC conjugated Phalloidin antibody were purchased from Invitrogen (Monza, Italia).

Synthesis of magnetic iron-substituted hydroxyapatite (FeHA). FeHA has been synthesized according to the method reported by Tampieri et al.¹⁷ Briefly, H₃PO₄ (44.4 g in 300 ml)

aqueous solution was added dropwise into basic aqueous suspension of Ca(OH)₂ (50.0 g in 400 ml) containing FeCl₂·4H₂O (12.7 g) and FeCl₃·6H₂O (17.9 g) as sources of Fe²⁺ and Fe³⁺ ions, under constant heating at 40 °C and stirring. The reaction product was kept in suspension by constant stirring and heating for 1 h after the neutralization reaction, and then left to age for 24 h at room temperature without further stirring. The precipitate was separated from mother liquor by centrifugation, then washed three times with water by centrifugation and finally freeze-dried and sieved at 150 μ m. ζ -potential was measured as a function of pH by an electroacoustic technique, using an electrokinetic sonic amplitude (ESA) measurement apparatus (Acoustosizer, Colloidal Dynamics, Sydney, Australia). A concentration of 1 vol% solid was used and the suspension, placed in the measurement cell, was kept under constant stirring at 25 °C. Automatic titration software was used to measure the potential as a function of pH (1 M HNO₃ and 1 M KOH were used to adjust the pH).

Synthesis of FeHA-PLLA micro-nanospheres. Poly(L-lactic) acid (PLLA)-FeHA micro-nanospheres were prepared by using the Pickering emulsion. Stable oil-in water emulsions were produced using the nano FeHA suspension as particulate emulsifier and the dichloromethane (CH₂Cl₂) solution of PLLA as oil phase. Aqueous dispersions of nano FeHA with solid content ranging from 0.001 to 0.030 wt% were prepared. Nano FeHA suspensions were treated with a probe sonicator, Ultrasonic Processor (UP50H, Hielscher, Germany) for 15 min to homogenize the dispersion, before the emulsion. The dispersions (50 g) were homogenized at 24000 rpm for 3 minutes with the CH₂Cl₂ solution of PLLA (5 g, 1.0 wt% solid content) at room temperature using a DIAX 600 (Heidolph, Kelheim, Germany). The spheres were formed via CH₂Cl₂ evaporation from the emulsions at 30 °C for 3 days. The sediment was repeatedly washed with water by centrifugation and freeze-dried at -60°C under vacuum (3 mbar) overnight for further characterization.

FeHA-PLLA micro-nanospheres characterizations. The X-ray diffraction (XRD) patterns of the samples were recorded with a D8 Advance Diffractometer (Bruker, Karlsruhe, Germany) equipped with a Lynx-eye position sensitive detector using Cu K α radiation (λ = 1.54178 Å) generated at 40 kV and 40 mA. XRD spectra were recorded in the 2 θ range from 10-60° with a step size (2 θ) of 0.02° and a counting time of 0.5 s. The infrared spectra were recorded in the wavelength range from 4000 to 400 cm⁻¹ with 2 cm⁻¹ resolution using a Nicolet 380 FT-IR spectrometer (Thermo Fisher Scientific Inc., Waltham, MA, US). A powdered sample (approximately 1 mg) was mixed with about 100 mg of anhydrous KBr. The mixture was pressed at 10 t pressure into 7 mm diameter discs. A pure KBr disk was used as blank. The thermal properties of the samples were measured using STA 449/C Jupiter (Netzsch, Germany). Simultaneous Thermal Gravimetric Analysis and Differential Scanning Calorimetry (TGA-DSC) were carried out in alumina crucibles from room temperature to 1200 °C at a heating rate of 10 °C/min in nitrogen flow. Morphological characterization of the samples was carried out by Scanning Electron Microscopy (SEM) using a Stereoscan 360 (Leica, Cambridge, UK) employing a secondary electron detector and an accelerating voltage of 15 kV and by Field Emission Gun Scanning Electron Microscopy (FEG-SEM) using a Sigma NTS GmbH (Carl Zeiss, Oberkochen, Germany). The speci-

mens were mounted on aluminum stubs using carbon tape and they were covered with a coating of Au using coating units Polaron Sputter Coater E5100 (Polaron Equipment, Watford, Hertfordshire, UK). Raman spectra were collected with a 800 nm focal length LabRam HR spectrograph (Jobin-Yvon, Horiba, Japan) using diffraction gratings of 600 lines/mm. The entrance slits were adjusted to 200 μm . The excitation laser beam (diode emitting at 532 nm) was focused through a 50x long-working distance objective (0.5 NA) into a 2 μm spot at the surface of the FeHA-coated spheres. A Peltier-cooled charge-couple device (CCD) (1064 x256 pixels) was used as detector. Raman spectra are the results of the signal averaging of at least three spectra with a spectral resolution better than 2 cm^{-1} . The Raman intensity units are counts per seconds (c.p.s.). Size and ζ -potential distributions of the FeHA-PLLA micro-nanospheres dispersed in water were measured by Dynamic Light Scattering (DLS) with a Zetasizer Nano ZS (Malvern Ltd., UK). For size distribution measurements, low-volume quartz cuvettes (105.251-QS, Hellma, Germany) were used. Ten runs of 30 seconds each were performed for each measurement and four measurements were carried out for each sample. ζ -potential was quantified by laser Doppler velocimetry as Electrophoretic Mobility using disposable electrophoretic cell (DTS1061, Malvern Ltd., UK). Twenty runs of 3 seconds each were collected in each measurement. Magnetization (M) of FeHA and FeHA-PLLA composites at low field was measured at $34 \times 10^{-4} \text{ N A}^{-1} \text{ m}^{-1}$ with a YSZ 01C/02C Susceptometer (Sartorius Mechatronics, Italy).

In vitro cell culture analysis. Mesenchymal stem cells (MSCs) isolated from the rabbit bone marrow were cultured in α -MEM medium plus 10% FBS and 1% Penicillin-Streptomycin (100 U/ml - 100 $\mu\text{g}/\text{ml}$), trypsinized, centrifuged and resuspended. MSCs were plated at a density of 3.0×10^3 cells/well in 96-well plates. 24 h after seeding, two different concentrations of FeHA-PLLA 1 wt% FeHA-PLLA 30 wt%, sterilized by 25 kGy γ -ray radiation, were added to the cell culture (500 $\mu\text{g}/\text{ml}$; 100 $\mu\text{g}/\text{ml}$). Cells were incubated under standard conditions (37°C, 5% CO_2) for 1, 4 and 7 days. Culture media was changed every other day. All cell-handling procedures were performed in a sterile laminar flow hood.

MTT assay. The MTT reagent was prepared at 5 mg/ml in 1x PBS. Cell were incubated with the MTT reagent 1:10 for 2 h at 37°C. Medium was collected and cells incubated with 200 μl of dimethyl sulfoxide for 15 min. In this assay, the metabolically active cells react with the tetrazolium salt in the MTT reagent to produce a formazan dye that can be observed at λ_{max} of 570 nm, using a Multiskan FC Microplate Photometer (Thermo Scientific). This absorbance is directly proportional to the number of metabolically active cells. Mean values of absorbance were determined. Five samples were analysed per group per time point.

Phalloidin immunofluorescence staining. Cells were washed with 1x PBS for 5 min, fixed with 4% (w/v) paraformaldehyde for 15 min and washed with 1x PBS for 5 min. Permeabilization was performed with 1x PBS with 0.1% (v/v) Triton X-100 for 5 min. FITC-conjugated Phalloidin antibody 1:500 in 1x PBS was added for 20 min at room temperature in the dark. Cells were washed with 1x PBS for 5 min and incubated with DAPI in 1x PBS for 5 min. Images were acquired by an In-

verted Ti-E fluorescence microscope (Nikon). One sample per group per time point was analyzed.

Statistical analysis. MTT results were expressed as $\text{MEAN} \pm \text{SEM}$ plotted on graph ($n=5$). Analysis of the effect of the application of FeHA-PLLA was made by two-way ANOVA, followed by Bonferroni's post-hoc test. Statistical analyses were performed by the GraphPad Prism software (version 5.0), with statistical significance set at $p \leq 0.05$.

Results and Discussion

Preparation of FeHA-PLLA micro-nanospheres. Superparamagnetic iron substituted hydroxyapatite (FeHA) nanocrystals to be used as particulate emulsifier for the preparation of the hybrid micro-nanospheres by Pickering emulsion were synthesized according to the procedure reported by Tampieri et al.¹⁷ Transmission electron microscopy (TEM) image revealed that they have needle-like morphology and nanometric dimensions in the range of 5-20 nm in width and 50-80 nm in length (Figure 1A).

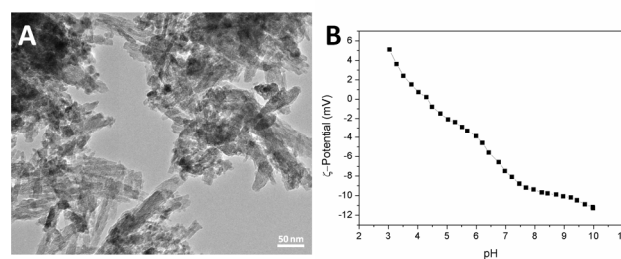


Figure 1. (A) TEM image of FeHA nanocrystals and (B) ζ -potential measured by acoustosizer of FeHA suspension as a function of pH.

Washing the nanocrystals twice with ultrapure water by centrifugation after the neutralization reaction, and re-dispersing them into ultrapure water a colloidal stable nano FeHA suspension was obtained. In this way the nanocrystals were not completely dried in order to avoid their aggregation. The ζ -potential of FeHA measured by acoustosizer from pH 3 to 10 (Figure 1B) showed positive values for $\text{pH} < 4$ (from 5 to 0 mV), whereas negative values have been found for the further increase of pH (from 0 to -12 mV). The point of zero charge (p.z.c.) was at pH around 4. Details of the other physicochemical properties of FeHA, are reported in table S1.

Aqueous suspensions of FeHA with solid contents of 0.001, 0.005, 0.010 and 0.030 wt% were prepared. These quantities were chosen to achieve ideal suspensions in terms of density (weak flocculation) and pH values (pH 6.5) for stable emulsions. In fact, previous works suggested that the emulsion is stabilized when the nanoparticles are weakly flocculated and in the case of hydroxyapatite when the pH is higher than 5. Below pH 5, hydroxyapatite tends to dissolve increasing the concentration of the ionic species and destabilize the emulsion.³³ FeHA has negative ζ -potential at pH 6.5 (-7 mV) indicating poor tendency to aggregate and suitable features to be used as nano-particulate emulsifier at this pH.

Stable oil in water (o/w) emulsions (conductivity $> 1 \mu\text{S cm}^{-1}$) were prepared by homogenizing the FeHA suspensions with PLLA in CH_2Cl_2 and four different FeHA-PLLA composites with different apatitic surface coverage amount (1, 5, 10, 30

wt%) were produced. The emulsion droplets of CH₂Cl₂ solution of PLLA were stabilized by the FeHA nanocrystals and the subsequent evaporation of CH₂Cl₂ leads to the formation of the magnetic hybrid organic-inorganic hollow microspheres. Neither pure aqueous suspensions nor suspensions with FeHA amount higher than 0.030 wt% produced stable emulsions.

Characterization of micro-nano FeHA-PLLA microspheres. Figure 2 shows the TGA profiles of pure FeHA (pattern a) and FeHA-PLLA micro-nano-spheres with four different apatitic surface coverage (patterns b, c, d and e). The FeHA percentage amount in the composites was calculated using equation (1):

$$FeHA \text{ amount (wt \%)} = \frac{R_{FeHA-PLLA} W_{lossFeHA}}{R_{FeHA}} + R_{FeHA-PLLA} \quad (1)$$

where $R_{FeHA-PLLA}$ is the residual amount of the composite at 1200 °C, $W_{lossFeHA}$ (10.5 wt%) and R_{FeHA} (89.5 wt%) are the weight loss and the residual amount of pure FeHA from room temperature to 1200 °C, respectively. Pure PLLA completely degraded at 1200 °C, whereas the weight loss of FeHA is due to the losses of the adsorbed and structural water and of the carbonate ions.

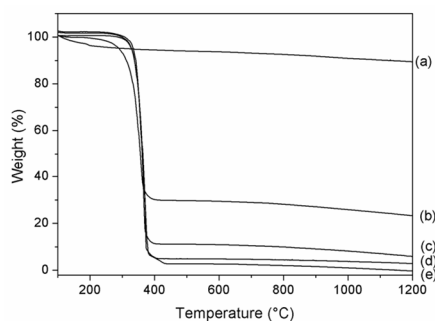


Figure 2. TGA curves of (a) FeHA and (b, c, d and e) FeHA-PLLA composites with four different FeHA surface coverage.

The FeHA loaded on the polymer was about 1, 5, 10 and 30 wt%. It is worth to notice that the initial weight percentage of FeHA relative to the polymeric phase was retained in the composites after the emulsion process, indicating that all the hydroxyapatite was bound to PLLA. Magnetic hydroxyapatite is dark brown colour due to the presence of Fe ions in the crystal lattice; therefore, FeHA-PLLA spheres displayed different colours from white to light brown as a function of the amount FeHA (Figure 3).

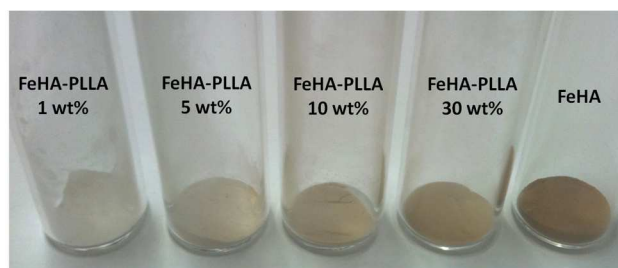


Figure 3. Photograph of magnetic FeHA-PLLA samples at different apatitic surface coverage.

Figure 4 shows the X-ray diffraction patterns of FeHA (a) and the FeHA-PLLA composites at different increasing amount of FeHA (patterns b, c, d and e).

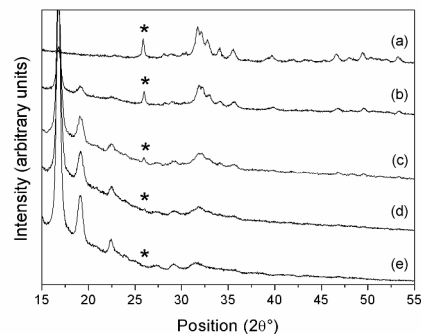


Figure 4. XRD patterns of (a) FeHA and FeHA-PLLA composites at four different FeHA surface coverage ((b) 30, (c) 10, (d) 5 and (e) 1 wt%). Asterisk indicates the (002) peak of FeHA.

The pattern of FeHA showed characteristic diffraction maxima of hydroxyapatite phase without the presence of any secondary phases (e.g. magnetite). The FeHA-PLLA diffraction patterns validated the increase of the FeHA content in the four composites. This finding is especially noticeable by the enhancement of the intensity of the reflections at $2\theta = 26^\circ$ and 32° attributed to the (002) and (211) hydroxyapatite planes, respectively (ICDD card No. 09-432). Moreover a clear enlargement of the full width at half maximum of the reflection at $19^\circ 2\theta$ (ascribed to the PLLA) as a function of the amount of FeHA can be distinguished. This result suggested that the crystallinity of the polymer could be reduced as a function of the amount of loaded nanoparticles. The crystallinity of bio-material (polymeric or inorganic) plays a very important role because it can influence its biological activity (towards cells), the kinetic of biodegradation and its physical and mechanical properties.³⁴ To estimate this structural parameter the crystalline melting temperature (T_m) of pure PLLA has been evaluated by Differential Scanning Calorimetry (DSC) and compared with those of the FeHA-PLLA composites (Table 1).

Table 1. Crystalline melting temperature (T_m) and full width at half maximum (FWHM) of the Raman peaks appearing at 395, 410 and 873 cm^{-1} and ascribed to the δCOO and $\nu\text{C-COO}$ vibrational modes of PLLA.

	T_m (°C)	FWHM (cm^{-1})		
		395 cm^{-1}	410 cm^{-1}	873 cm^{-1}
PLLA	164.5	8.9	8.6	7.3
FeHA-PLLA 1 wt%	166.4	7.9	5.7	6.7
FeHA-PLLA 5 wt%	165.2	8.1	6.1	7.0
FeHA-PLLA 10 wt%	164.6	8.3	6.2	7.0
FeHA-PLLA 30 wt%	164.1	12.7	10.2	8.3

The T_m increased for the composite loaded with up to 1 wt % of FeHA, while it progressively decreased in the composites loaded with higher amount of FeHA. The FeHA-PLLA 30 wt% composite showed a T_m slightly lower than that of pure PLLA. Small amount of FeHA acted as nucleating agent and promoted the PLLA crystallization, whilst a further increase of FeHA can disrupt the regularity of the PLLA chain structure. The same scenario has been observed by other authors in the preparation of PLLA/TiO₂ nano-composites.³⁵

Figure 5 shows the Raman spectra of FeHA (a) and the FeHA-PLLA composites (b-e). The spectrum of FeHA displayed the main peak at ca. 960 cm⁻¹ ascribed to the symmetric stretching (ν_1) of the phosphate groups.³⁶ The spectra of the composites also displayed a weak peak at ca. 960 cm⁻¹, which increased its intensity as a function of the apatite amount added in the emulsion. Hence, the Raman spectra of the FeHA-PLLA confirmed the increase of the apatite content in the samples, validating the TGA and XRD analyses.

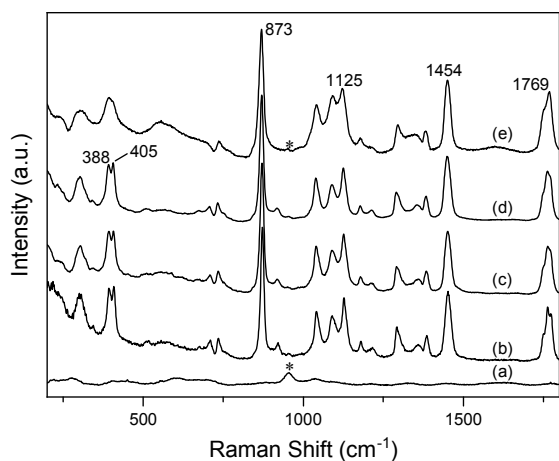


Figure 5. Raman spectra of FeHA (a) and FeHA-PLLA composites at four different FeHA surface coverage ((b) 30, (c) 10, (d) 5 and (e) 1 wt%). Asterisk marks the peak of the symmetric stretching of the phosphate groups of FeHA.

The width of the peaks at ca. 873 and 410 cm⁻¹ ascribed to the ν C-COO and 395 cm⁻¹ due to the δ CCO of PLLA is very sensitive to the crystallinity degree of the PLLA.³⁷ Indeed, the full widths at half maximum (FWHM) of these peaks for the pure PLLA and for the FeHA-PLLA composites are shown in Table 1. The FWHM values of the three peaks decrease in the composite loaded with 1 wt % of FeHA in comparison with the pure PLLA, while they increase for the further loading with higher amount of FeHA. These results are completely in agreement with the DSC analyses indicating that the crystallinity of the FeHA-PLLA 1 wt% is higher than pure PLLA but it is gradually reduced when adding higher quantity of FeHA.

FTIR spectroscopy has been also used to obtain a complete structural analysis of the composites. The spectrum of pure PLLA (Figure S1A) fits with that of semi-crystalline PLLA.³⁸ The spectra of the FeHA-PLLA composites show also peaks at ca. 1780, 1032, 565 and 601 cm⁻¹ (Figure S1A). The presence of a shoulder at 1780 cm⁻¹ could be related to the stretching vibrations (ν C=O) of the PLLA carbonyl groups, interacting with the apatitic calcium and iron positive ions, confirming the already reported assumption²⁹ (Figure S1B). The other

peaks are related to the FeHA nanocrystals covering the PLLA. The increased amount of FeHA in the composites is also witnessed by the enhancement of the relative intensity of the apatitic band at 1032 cm⁻¹.

Figure 6 shows the Scanning Electron Microscopy (SEM) micrographs of the FeHA-PLLA composites at different FeHA surface coverage. Free FeHA nanoparticles were not observed on the background of SEM images, and on this basis it could be evaluated that all the apatite was attached on the PLLA. The samples showed differences in terms of size distribution. A spherical shape was maintained in all samples, while it is clear that the increase of the FeHA decreases the mean size of the spheres. This finding can be explained because the growth of inorganic phase amount on the surface increases the PLLA shrinkage tension, reducing the particles dimensions. All the samples showed a good dimensional range from about 2 μ m for FeHA-PLLA 1 wt% to about 500 nm for FeHA-PLLA 30 wt%.

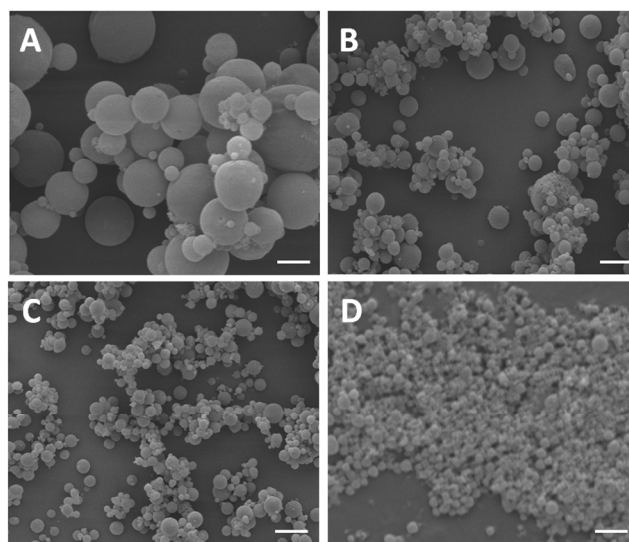


Figure 6. SEM images of FeHA-PLLA composites at different FeHA surface coverage ((A) 1, (B) 5, (C) 10 and (D) 30 wt%). Scale bars are 2 μ m.

The surface texture of the sample has been investigated by Field Emission Gun Scanning Electron Microscopy (FEG-SEM) analyses (Figure 7). Some small holes are clearly visible on the surface (especially in the biggest spheres), demonstrating that the spheres are hollow. The increase of the FeHA nanocrystals attached to PLLA was evident indicating good affinity of the inorganic phase for the polymeric one.

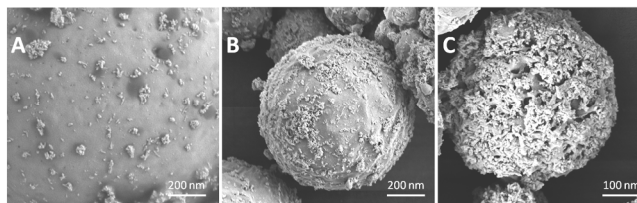


Figure 7. FEG-SEM images of the surface of (A) FeHA-PLLA 1 wt%, (B) FeHA-PLLA 10 wt% and (C) FeHA-PLLA 30 wt%.

The diameter distribution of the spheres suspended in ultrapure water was measured by Dynamic Light Scattering (DLS) (Table 2). The mean size of the FeHA nanoparticles was 96 nm. This value was not observed in the size distributions of the microspheres confirming that FeHA nanoparticles were firmly attached on the PLLA surface even in aqueous suspensions. Moreover, the values of the dimensions as well as the reduction of the size of the composites as a function of the FeHA amount observed by DLS is in complete agreement with the SEM observations.

Table 2. Chemical-physical features of FeHA and FeHA-PLLA micro-nanospheres with different FeHA surface coverage amount.

Sample	Size Distribution (nm) ^[a]	ζ-Potential (mV) (pH 6.5) ^[a]	Magnetic moment (emu/g) ^[b]
FeHA	96.0 ± 32.6	-7.9 ± 2.0	0.391 ± 0.011
FeHA-PLLA 1 wt%	1837.0 ± 298.0	-30.7 ± 3.5	-
FeHA-PLLA 5 wt%	633.6 ± 101.6	-23.2 ± 4.2	0.011 ± 0.001
FeHA-PLLA 10 wt%	497.8 ± 63.3	-14.1 ± 3.2	0.035 ± 0.002
FeHA-PLLA 30 wt%	301.9 ± 52.1	-8.9 ± 2.1	0.121 ± 0.003

^[a] Measured by DLS; ^[b] Measured by susceptometry at low magnetic field.

The surface charge of the micro-nano-spheres is a very important parameter since it affects their stability in suspensions and can be useful to evaluate the chemical interactions of biomolecules on the surface. Moreover, the surface charge of the carrier plays a fundamental role in their interaction with cells.³⁹ The ζ-potential of the PLLA is negative due to the its negatively charged -C=O surface groups (about -30 mV).²⁹ As discussed above from FTIR results, the polymeric -C=O surface groups can interact with the positively charged calcium and iron surface ions of the FeHA nanoparticles neutralizing the negative charge. Hence, this interaction can explain the surface charge reduction as a function of the increasing of the FeHA amount loaded on the surface of the spheres (from -30.7 to -8.9 mV) (Table 2). It is worth to be highlighted that the ζ-potential of the FeHA-PLLA 30 wt% is very close to the value of the FeHA indicating a high degree of surface coverage by the inorganic phase.

The magnetization measurements showed a linear increase of the composite magnetic features (magnetic moment per unit volume) as a function of the FeHA amount (Table 2, Figure S2). This graph could be used as a sort of calibration curve, to select the quantity of FeHA to be bound to PLLA to tailor the final magnetization of the composite. No magnetization signal has been detected in the sample with 1 wt% of FeHA due to the low quantity of magnetic phase. The magnetic moment per unit volume of FeHA-PLLA 30 wt% was similar to the values measured by Bock et al.⁴⁰ and Tampieri et al.⁴¹ in magnetic

scaffolds made of collagen-hydroxyapatite impregnated with ferrofluids containing iron oxide nanoparticles coated with various biopolymers and with magnetite nanoparticles, respectively.

In vitro analysis of biocompatibility and cell morphology. For the preliminary *in vitro* cell culture analysis, the selected experimental groups were FeHA-PLLA 1 wt% and FeHA-PLLA 30 wt% due to their significant differences in terms of dimension and FeHA amount loaded on the polymer. Bone marrow mesenchymal stem cells (MSCs) were used, since these cells are highly sensitive to material toxicity and reproduce closely a possible clinical set application.⁴²

In a previous study the complete biocompatibility of FeHA *in vitro* and *in vivo* have been demonstrated.¹⁸ FeHA, at even with very high FeHA concentration (2000 µg/ml), did not reduce cell proliferation and none toxic effects were seen on cell culture. Moreover, the biocompatibility of PLLA is well known, in fact, this polymer is commonly used as material for the preparation of biomedical devices.³⁴

In this study we focused on the comparison between FeHA-PLLA 1 wt% and FeHA-PLLA 30 wt% in order to evaluate firstly the biocompatibility of these new systems and subsequently how dimension and FeHA amount could influence cell behavior. MSCs were cultured in the presence of 100 µg/ml and 500 µg/ml of FeHA-PLLA 1 wt% and FeHA-PLLA 30 wt% for 1, 4 and 7 days. The quantification of metabolically active cells for each time point was performed by use of the MTT assay, as shown in figure 8.

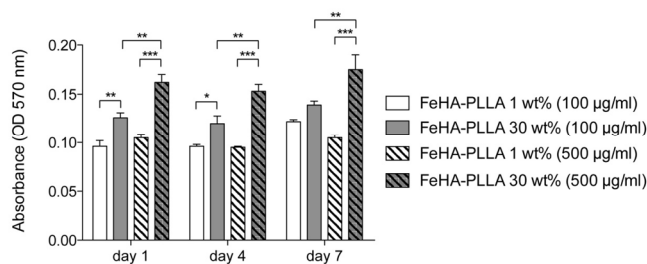


Figure 8. Analysis of cell proliferation by the MTT assay, after 1, 4 and 7 days MSCs incubation period with FeHA-PLLA 1 wt% and FeHA-PLLA 30 wt%. * $p \leq 0.05$, ** $p \leq 0.01$, *** $p \leq 0.001$, $n = 5$.

The results showed that FeHA-PLLA 30 wt% enhanced cell proliferation respect to FeHA-PLLA 1 wt%. In detail, at lower concentration a significant difference was seen at day 1 and day 4 ($p \leq 0.01$ and $p \leq 0.05$ respectively); at higher concentration the difference was even larger at every time points ($p \leq 0.001$). It is also remarkable how the higher concentration (500 µg/ml) strongly influenced cells behavior respect to the lower concentration (100 µg/ml) only with FeHA-PLLA 30 wt% sample ($p \leq 0.01$ at every time points). However, all the groups did not reduce cell proliferation confirming the total biocompatibility of the samples and that the toxic CH_2Cl_2 , used as solvent, was completely removed during the synthesis of FeHA-PLLA micro-nanospheres.

This data, in agreement with those previously obtained,¹⁸ demonstrated that cells are positively affected by the presence

of FeHA in the culture media. Looking at the proliferation of each sample, it is seen that cells did not proliferate so much from day 1 to day 7 probably due the high concentration and dimension of the particles ranging from 500 nm up to 2 μm in the culture media. However analyzing the cell morphology at each time point by phalloidin, a specific marker for actin filaments, characteristic MSCs morphology were observed between groups (Figures 9 A,C). MSCs were nicely distributed with their characteristic morphology and no differences were observed between groups. Looking in detail at the cell morphology, FeHA-PLLA particles were seen accumulated in the cytoplasm (Figures 9 B,D) and even when the cells showed high FeHA-PLLA particles accumulation they remained firmly attached to the well surface. This fact suggests that the novel intrinsically magnetic FeHA-PLLA spheres were well tolerated by the cells. Finally, in line with the previous results obtained with FeHA nanoparticles, the valuable potential biomedical applications of FeHA-PLLA composites were assessed. Moreover, due to their superparamagnetic properties, further works will be carried out to explore a possible enhanced cell behaviour in presence of magnetic field.

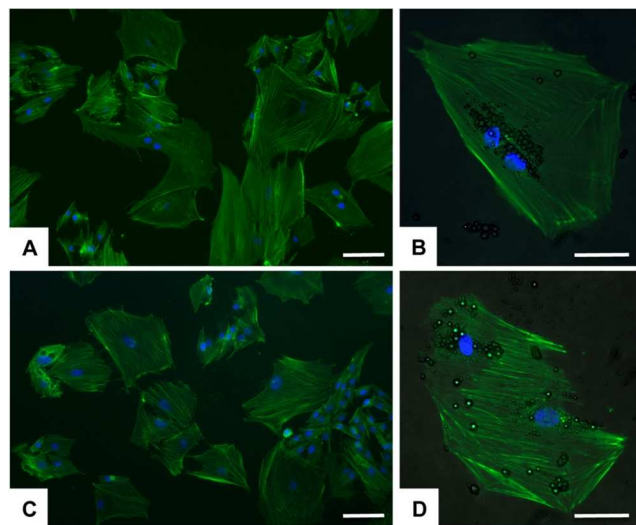


Figure 9. Analysis of cell morphology. MSCs were spread with good morphology and firmly attached to the surface. (A, B) FeHA-PLLA 1 wt% and FeHA-PLLA 30 wt% at day 3 respectively. (C, D) Enlargement of spread cell. Black spots are FeHA-PLLA 1 wt% and FeHA-PLLA 30 wt% respectively that have been internalized by cells. Phalloidin in green stains for actin filaments and DAPI in blue stains for cell nuclei. Scale bars: (A, C) 100 μm , (B, D) 50 μm .

Conclusions

Bioactive and biodegradable magnetic hollow FeHA nanocrystals coated poly(L-lactic acid) (PLLA) micro-nanospheres with potential uses as building block material for the preparation of magnetic scaffold for hard tissue regeneration as well as nanocarriers of biomolecules to be guided inside the body by an external magnetic field were produced using the Pickering emulsion. Varying the amount of FeHA (from 1 to 30 wt %), the chemical-physical features of the hybrid beads such as size, surface charge and magnetization can be tailored. The hybrid composite with the highest amount of inorganic phase displayed the lowest dimension and the highest surface charge and magnetization. All the samples did not affect the bone

marrow mesenchymal stem cells viability or morphology, exhibiting a good level of biocompatibility. Moreover, the spheres coated with the higher amount of FeHA revealed the better cell proliferation than those coated with lower amount. The possibility to tailor the amount of FeHA in the composites will be very helpful to improve their good biological performance to respond to wide specific needs in medical applications. In addition, this work open new perspectives in the use of FeHA as biocompatible and biodegradable magnetic biomaterial in alternative to the current magnetic phases used in medicine whose biodegradability, toxicity of degradation by-products and long-term effects in the human body are not yet completely assessed.

ASSOCIATED CONTENT

Supporting Information. Compositional features and specific surface area (SSA_{BET}) of FeHA. FTIR spectra of PLLA and FeHA-PLLA composites. Magnetization of the FeHA-PLLA composites as function of FeHA percentage amount attached. This material is available free of charge via the Internet at <http://pubs.acs.org>.

AUTHOR INFORMATION

Corresponding Author

*Dr. Michele Iafisco. E-mail: michele.iafisco@istec.cnr.it

Author Contributions

The manuscript was written through contributions of all authors. All authors have given approval to the final version of the manuscript.

ACKNOWLEDGMENT

MI, MS, SP and AT acknowledge the European project SMILEY (FP7-NMP-2012-SMALL-6-310637). JMDL and JGM acknowledge the project CRYSFUNBIO (MAT2011-28543) and Factoría de Cristalización (Consolider Ingenio 2010) of the Spanish MINECO.

REFERENCES

- Colombo, M.; Carregal-Romero, S.; Casula, M. F.; Gutierrez, L.; Morales, M. P.; Bohm, I. B.; Heverhagen, J. T.; Prospero, D.; Parak, W. J., Biological applications of magnetic nanoparticles. *Chemical Society Reviews* **2012**, 41, (11), 4306-4334.
- Liu, J.; Qiao, S. Z.; Hu, Q. H.; Lu, G. Q., Magnetic Nanocomposites with Mesoporous Structures: Synthesis and Applications. *Small* **2011**, 7, (4), 425-443.
- Sensenig, R.; Sapir, Y.; MacDonald, C.; Cohen, S.; Polyak, B., Magnetic nanoparticle-based approaches to locally target therapy and enhance tissue regeneration in vivo. *Nanomedicine* **2012**, 7, (9), 1425-1442.
- Xu, C.; Miranda-Nieves, D.; Ankrum, J. A.; Matthiesen, M. E.; Phillips, J. A.; Roes, I.; Wojtkiewicz, G. R.; Juneja, V.; Kultima, J. R.; Zhao, W.; Vemula, P. K.; Lin, C. P.; Nahrendorf, M.; Karp, J. M., Tracking Mesenchymal Stem Cells with Iron Oxide Nanoparticle Loaded Poly(lactide-co-glycolide) Microparticles. *Nano Letters* **2012**, 12, (8), 4131-4139.
- Béalle, G.; Di Corato, R.; Kolosnjaj-Tabi, J.; Dupuis, V.; Clément, O.; Gazeau, F.; Wilhelm, C.; Ménager, C., Ultra Magnetic Liposomes for MR Imaging, Targeting, and Hyperthermia. *Langmuir* **2012**, 28, (32), 11834-11842.
- Yao, W.; Wen, J.; Xiantao, W.; Bin, H.; Xiaobo, Z.; Gang, W.; Zhongwei, G., A novel calcium phosphate ceramic-magnetic nanoparticle composite as a potential bone substitute. *Biomedical Materials* **2010**, 5, (1), 015001.
- Panseri, S.; Cunha, C.; D'Alessandro, T.; Sandri, M.; Russo, A.; Giavaresi, G.; Maracci, M.; Hung, C. T.; Tampieri, A.,

Magnetic Hydroxyapatite bone substitutes to enhance tissue regeneration: Evaluation in vitro using osteoblast-like cells and in vivo in a bone defect. *PLoS ONE* **2012**, *7*, (6).

8. Wei, Y.; Zhang, X.; Song, Y.; Han, B.; Hu, X.; Wang, X.; Lin, Y.; Deng, X., Magnetic biodegradable Fe₃O₄/CS/PVA nanofibrous membranes for bone regeneration. *Biomedical Materials* **2011**, *6*, (5), 055008.

9. Meng, J.; Zhang, Y.; Qi, X.; Kong, H.; Wang, C.; Xu, Z.; Xie, S.; Gu, N.; Xu, H., Paramagnetic nanofibrous composite films enhance the osteogenic responses of pre-osteoblast cells. *Nanoscale* **2010**, *2*, (12), 2565-2569.

10. Amstad, E.; Textor, M.; Reimhult, E., Stabilization and functionalization of iron oxide nanoparticles for biomedical applications. *Nanoscale* **2011**, *3*, (7), 2819-2843.

11. Rosen, J. E.; Chan, L.; Shieh, D.-B.; Gu, F. X., Iron oxide nanoparticles for targeted cancer imaging and diagnostics. *Nanomedicine: Nanotechnology, Biology and Medicine* **2012**, *8*, (3), 275-290.

12. Almeida, J. P. M.; Chen, A. L.; Foster, A.; Drezek, R., In vivo biodistribution of nanoparticles. *Nanomedicine* **2011**, *6*, (5), 815-835.

13. Mahmoudi, M.; Hofmann, H.; Rothen-Rutishauser, B.; Petri-Fink, A., Assessing the In Vitro and In Vivo Toxicity of Superparamagnetic Iron Oxide Nanoparticles. *Chemical Reviews* **2012**, *112*, (4), 2323-2338.

14. Yigit, M. V.; Moore, A.; Medarova, Z., Magnetic Nanoparticles for Cancer Diagnosis and Therapy. *Pharmaceutical Research* **2012**, *29*, (5), 1180-1188.

15. Seeney, C.; Ojwang, J. O.; Weiss, R. D.; Klostergaard, J., Magnetically vectored platforms for the targeted delivery of therapeutics to tumors: history and current status. *Nanomedicine* **2012**, *7*, (2), 289-299.

16. Ghosh Chaudhuri, R.; Paria, S., Core/Shell Nanoparticles: Classes, Properties, Synthesis Mechanisms, Characterization, and Applications. *Chemical Reviews* **2011**, *112*, (4), 2373-2433.

17. Tampieri, A.; D'Alessandro, T.; Sandri, M.; Sprio, S.; Landi, E.; Bertinetti, L.; Panseri, S.; Peponi, G.; Goettlicher, J.; Bañobre-López, M.; Rivas, J., Intrinsic magnetism and hyperthermia in bioactive Fe-doped hydroxyapatite. *Acta Biomaterialia* **2012**, *8*, (2), 843-851.

18. Panseri, S.; Cunha, C.; D'Alessandro, T.; Sandri, M.; Giavaresi, G.; Marcacci, M.; Hung, C. T.; Tampieri, A., Intrinsically superparamagnetic Fe-hydroxyapatite nanoparticles positively influence osteoblast-like cell behaviour. *Journal of Nanobiotechnology* **2012**, *10*.

19. Wei, G.; Ma, P. X., Structure and properties of nano-hydroxyapatite/polymer composite scaffolds for bone tissue engineering. *Biomaterials* **2004**, *25*, (19), 4749-4757.

20. Wang, H.; Leeuwenburgh, S. C. G.; Li, Y.; Jansen, J. A., The use of micro- and nanospheres as functional components for bone tissue regeneration. *Tissue Engineering - Part B: Reviews* **2012**, *18*, (1), 24-39.

21. Pickering, S. U., CXCVI.-Emulsions. *Journal of the Chemical Society, Transactions* **1907**, *91*, 2001-2021.

22. Larson-Smith, K.; Pozzo, D. C., Pickering Emulsions Stabilized by Nanoparticle Surfactants. *Langmuir* **2012**, *28*, (32), 11734-11741.

23. Morse, A. J.; Dupin, D.; Thompson, K. L.; Armes, S. P.; Ouzineb, K.; Mills, P.; Swart, R., Novel Pickering Emulsifiers based on pH-Responsive Poly(tert-butylaminoethyl methacrylate) Latexes. *Langmuir* **2012**, *28*, (32), 11742-11753.

24. Okada, M.; Maeda, H.; Fujii, S.; Nakamura, Y.; Furuzono, T., Formation of Pickering Emulsions Stabilized via Interaction between Nanoparticles Dispersed in Aqueous Phase and Polymer End Groups Dissolved in Oil Phase. *Langmuir* **2012**, *28*, (25), 9405-9412.

25. Marku, D.; Wahlgren, M.; Rayner, M.; Sjöo, M.; Timgren, A., Characterization of starch Pickering emulsions for potential applications in topical formulations. *International Journal of Pharmaceutics* **2012**, *428*, (1-2), 1-7.

26. Li, W.; Yu, L. J.; Liu, G. P.; Tan, J. J.; Liu, S. Y.; Sun, D. J., Oil-in-water emulsions stabilized by Laponite particles modified with short-chain aliphatic amines. *Colloids and Surfaces a-Physicochemical and Engineering Aspects* **2012**, *400*, 44-51.

27. Bourgeat-Lami, E.; Farzi, G. A.; David, L.; Putaux, J. L.; McKenna, T. F. L., Silica Encapsulation by Miniemulsion Polymerization: Distribution and Localization of the Silica Particles in Droplets and Latex Particles. *Langmuir* **2012**, *28*, (14), 6021-6031.

28. Zoppe, J. O.; Venditti, R. A.; Rojas, O. J., Pickering emulsions stabilized by cellulose nanocrystals grafted with thermoresponsive polymer brushes. *Journal of Colloid and Interface Science* **2012**, *369*, 202-209.

29. Iafisco, M.; Palazzo, B.; Ito, T.; Otsuka, M.; Senna, M.; Delgado-Lopez, J.; Gomez-Morales, J.; Tampieri, A.; Prat, M.; Rimondini, L., Preparation of core-shell poly(l-lactic) acid-nanocrystalline apatite hollow microspheres for bone repairing applications. *Journal of Materials Science: Materials in Medicine* **2012**, *23*, (11), 2659-2669.

30. Suggs, L.; Moore, S.; Mikos, A., Synthetic Biodegradable Polymers for Medical Applications

Physical Properties of Polymers Handbook. In Mark, J. E., Ed. Springer New York: 2007; pp 939-950.

31. Bigall, N. C.; Wilhelm, C.; Beoutis, M.-L.; Garcia-Hernandez, M.; Khan, A. A.; Giannini, C.; Sanchez-Ferrer, A.; Mezzenga, R.; Matera, M. E.; Garcia, M. A.; Gazeau, F.; Bittner, A. M.; Manna, L.; Pellegrino, T., Colloidal Ordered Assemblies in a Polymer Shell - A Novel Type of Magnetic Nanobeads for Theranostic Applications. *Chemistry of Materials* **2013**.

32. Chiang, W.-L.; Ke, C.-J.; Liao, Z.-X.; Chen, S.-Y.; Chen, F.-R.; Tsai, C.-Y.; Xia, Y.; Sung, H.-W., Pulsatile Drug Release from PLGA Hollow Microspheres by Controlling the Permeability of Their Walls with a Magnetic Field. *Small* **2012**, *8*, (23), 3584-3588.

33. Gómez-Morales, J.; Iafisco, M.; Delgado-López, J. M.; Sarda, S.; Drouet, C., Progress on the preparation of nanocrystalline apatites and surface characterization: Overview of fundamental and applied aspects. *Progress in Crystal Growth and Characterization of Materials* **2013**, *59*, (1), 1-46.

34. Saeidlou, S.; Huneault, M. A.; Li, H.; Park, C. B., Poly(lactic acid) crystallization. *Progress in Polymer Science* **2012**, *37*, (12), 1657-1677.

35. Buzarovska, A.; Grozdanov, A., Biodegradable poly(L-lactic acid)/TiO₂ nanocomposites: Thermal properties and degradation. *Journal of Applied Polymer Science* **2012**, *123*, (4), 2187-2193.

36. Delgado-López, J. M.; Iafisco, M.; Rodríguez, I.; Tampieri, A.; Prat, M.; Gómez-Morales, J., Crystallization of bioinspired citrate-functionalized nanoapatite with tailored carbonate content. *Acta Biomaterialia* **2012**, *8*, (9), 3491-3499.

37. Smith, P. B.; Leugers, A.; Kang, S.; Yang, X.; Ling Hsu, S., Raman characterization of orientation in poly(lactic acid) films. *Macromolecular Symposia* **2001**, *175*, (1), 81-94.

38. Kister, G.; Cassanas, G.; Vert, M., Effects of morphology, conformation and configuration on the IR and Raman spectra of various poly(lactic acid)s. *Polymer* **1998**, *39*, (2), 267-273.

39. Verma, A.; Stellacci, F., Effect of Surface Properties on Nanoparticle-Cell Interactions. *Small* **2010**, *6*, (1), 12-21.

40. Bock, N.; Riminucci, A.; Dionigi, C.; Russo, A.; Tampieri, A.; Landi, E.; Goranov, V. A.; Marcacci, M.; Dediu, V., A novel route in bone tissue engineering: Magnetic biomimetic scaffolds. *Acta Biomaterialia* **2010**, *6*, (3), 786-796.

41. Tampieri, A.; Landi, E.; Valentini, F.; Sandri, M.; D'Alessandro, T.; Dediu, V.; Marcacci, M., A conceptually new type of bio-hybrid scaffold for bone regeneration. *Nanotechnology* **2011**, *22*, (1), 015104.

42. Baksh, D.; Song, L.; Tuan, R. S., Adult mesenchymal stem cells: characterization, differentiation, and application in cell and gene therapy. *Journal of Cellular and Molecular Medicine* **2004**, *8*, (3), 301-316.

Bioactive and biodegradable magnetic hollow micro-nanospheres (from 2 μm to 500 nm) made of polymeric shell of poly(L-lactic) acid coated with iron doped hydroxyapatite (FeHA) are produced by Pickering emulsion. The FeHA amount can be tailored to modify their chemical-physical features (e. g. size, polymer crystallinity, surface charge and magnetization) as well as the bone related cell proliferation.

